Path-dependent Volatility: An Application to the South African Market

Shivan Sookdeo

A dissertation submitted to the Faculty of Commerce, University of Cape Town, in partial fulfilment of the requirements for the degree of Master of Philosophy.

October 4, 2017

MPhil in Mathematical Finance,
University of Cape Town.

Declaration

I declare that this dissertation is my own, unaided work. It is being submitted for the Degree of Master of Philosophy in the University of the Cape Town. It has not been submitted before for any degree or examination in any other University.

_____

October 4, 2017

Abstract

Industry and academia have thus far focussed on three classes of volatility models, namely, constant volatility, local volatility and stochastic volatility. Path-dependent volatility models are a lesser known class of models which possess the key characteristic of completeness together with the ability to generate a wide range of volatility dynamics with respect to the underlying asset (Guyon, 2014). This dissertation highlights the usefulness and practicality of these models for application in the South African market, while drawing comparisons with other widely used models. The tests cover both pricing and hedging of vanilla European options on the FTSE JSE Top 40. The Black-Scholes, Heston and CEV models are used as comparative benchmarks for each of the other classes of models.

Acknowledgements

I would like to thank my supervisor, Dr. Johan de Kock, for his guidance and insight throughout the progression of this dissertation. I would also like to thank my family for their unwavering support throughout my academic career. In addition, I would like to thank Prof. David Taylor and the mathematical finance team at the University of Cape Town for the support provided over the year.

Contents

List of Figures

List of Tables

Chapter 1

Introduction

Diffusion models of assets involve two key parameters, the first being the drift component and the second being the volatility component. Thus far, three broad categories of models have featured in industry and academia namely, constant volatility (CV) models, local volatility (LV) models and stochastic volatility (SV) models. CV models include early models by Bachelier and the widely used Black-Scholes model (Black and Scholes, 1973). They are the simplest models to calibrate and use practically, however, they suffer a number of pitfalls. LV models were introduced by Dupire *et al.* (1994) and yield arbitrage free prices for a given volatility smile. SV models allow volatility to be random in nature and include extra Brownian motions to achieve this. Examples of these include the Heston and SABR models.

A key characteristic for an option pricing model is completeness, i.e. the ability to yield unique prices for contingent claims independent of any utility or preferences (Guyon, 2014). Dupire *et al.* (1994) argue that completeness is most valuable as it allows for arbitrage free pricing and hedging. CV and LV models are complete, however, SV models are not. Another key feature of empirical data is the spot-vol dynamics which constant volatility models lack. This is evident in the volatility smiles observed in the market which indicate volatility being dependent on the underlying asset price, while constant volatility models do not reflect this feature. SV models have the ability to encapsulate rich spot-volatility dynamics, however, this comes at the cost of completeness.

Guyon (2014) shows that path-dependent volatility (PDV) models combine benefits from both LV and SV models. They are complete models and are able to generate an even wider range of spot-volatility dynamics than SV models. For this reason, Guyon (2014) argues that the lack of attention from industry and academia paid to PDV models compared to SV and LV models is unfair. This dissertation seeks to explore and apply PDV models to a South African setting, testing the usefulness of the model for industry products.

This dissertation is organised as follows. Chapter 2 provides an overview of

the different classes of models, together with the advantages and disadvantages of each class. Chapter 3 details the calibration of the selected models including the Black-Scholes constant volatility model, Heston stochastic volatility model, CEV local volatility model and finally the PDV model. In chapter 4, the PDV models are tested using vanilla European options on the JSE FTSE Top 40. The first test involves the pricing of these instruments, while the second test involves hedging. As an extension, a comparison of model generated prices for forward starting options is included. Lastly chapter 5 concludes with a discussion of the results and suggestions for extensions.

Chapter 2

Classes of Models

This chapter consists of a brief background and literature review of each of the classes of models. This begins with the constant volatility models, followed by local and stochastic volatility models. Finally, the path-dependent volatility models are discussed, together with the hybrid extensions and generalisations of the models.

2.1 Constant Volatility Models

The Black-Scholes model is used widely in industry for both pricing and hedging of derivatives, often with prices being quoted in terms of the implied volatility based on the model (Hobson and Rogers, 1998). The development of this model has been the cornerstone of modern financial engineering (Hull, 2006). Under the risk neutral measure, the underlying asset follows a geometric Brownian motion given by

$$dS_t = rS_t dt + \sigma S_t dW_t \,,$$

where S_t denotes the value of the underlying asset at time t, r denotes the risk-free rate, σ denotes the constant volatility and W_t is a Wiener process (Black and Scholes, 1973). Under these dynamics, the underlying asset is log-normally distributed, and hence the returns of the asset are normally distributed. An advantage of this model is the availability of closed form analytical prices for vanilla European call and put options, as well as simple exotic options (Hull, 2006). This model has also been applied to pricing corporate debt (Merton, 1973).

However, empirical data shows that volatility of stocks is not constant and the prices at which derivatives are traded are inconsistent with a constant volatility assumption (Hobson and Rogers, 1998). This was most evident after the market crash of 1987, and this led to the development of more realistic models (Foschi and Pascucci, 2008). Prior to the 1987 market crash the volatility surface of equity index options was indeed flat, however, this is no longer true and the volatility smile

phenomenon has spread to other markets such as interest rate options and currency options (Derman, 2003). Hagan *et al.* (2002) note that the mismatch with a strike independent volatility is most critical for fixed income and foreign exchange desks which typically have exposures over a wide range of strikes. Constant volatility models also did not cater for the emergence of exotic options and structured products which incorporated several different strikes and future levels of volatility (Derman, 2003).

2.2 Local Volatility Models

In order to cater for the observed volatility smiles, LV models attempt to calibrate prices to the smile by allowing the volatility to vary. Under a LV model, the dynamics of the underlying assets takes the form

$$dS_t = rS_t dt + \sigma(S_t, t)S_t dW_t \,,$$

which illustrates that the volatility is a deterministic function of the spot price (Dupire *et al.*, 1994). This model is complete with attainable contingent claims and a unique equivalent martingale measure (Harrison and Pliska, 1981). Dumas *et al.* (1998) empirically show that LV models do not perform well for hedging purposes compared to the standard Black-Scholes model. Hagan *et al.* (2002) attributes this under-performance to the LV models incorrect prediction of volatility skew movements which are inconsistent with reality and the Black-Scholes model. LV models predict that the volatility smile shifts to lower prices when the underlying price increases, however, empirical evidence shows that the volatility smile and the underlying price move in the same direction (Hagan *et al.*, 2002). Foschi and Pascucci (2008) also note the need to be continuously re-calibrated as a well-known drawback of these models.

The constant elasticity of variance (CEV) model is a widely used parametric LV model (Linetsky and Mendoza, 2010). Under the CEV model the dynamics of the underlying is given as:

$$dS_t = rS_t dt + \sigma S_t^{\alpha} dW_t \,.$$

The local volatility function is therefore

$$\sigma(S_t, t) = \sigma S_t^{\alpha - 1} \,,$$

and is independent of time. For certain values of α, the process reduces down to special cases:

- $\alpha = 1$: Geometric Brownian motion
- $\alpha = \frac{1}{2}$: Square-root, or Cox - Ingersol - Ross (CIR), process without mean reversion
- $\alpha = 0$: Ornstein-Uhlenbeck process without mean reversion

2.3 Stochastic Volatility Models

In general a SV model defines two stochastic processes, one for the underlying asset and one for the variance, $V_t = \sigma_t^2$:

$$dS_t = \phi S_t dt + \sigma_t S_t dW t$$

and

$$dV_t = \mu V_t dt + \epsilon V_t dZ_t \,,$$

where ϕ may be a function of S, σ and t, μ and ϵ may depend on σ and t and the Brownian motions have correlation ρ (Hull and White, 1987). Romano and Touzi (1997) show that markets in SV models are incomplete and it is not possible to hedge the risk for a given contingent claim using the underlying asset. One of the reasons for this incompleteness is that volatility is not a traded instrument, and there is no asset which is instantaneously perfectly correlated to V_t (Hull and White, 1987).

The Heston model is a prominent example of a SV model. It assumes the following dynamics for the underlying asset and the instantaneous variance:

$$dS_t = rS_t dt + \sqrt{\nu_t} S_t dW_t^S$$

and

$$d\nu_t = \kappa(\theta - \nu_t)dt + \sigma\sqrt{\nu_t} dW_t^\nu \,,$$

where the Brownian motions have correlation ρ (Heston, 1993). This model is amenable to Fourier transform pricing and has been applied to derivatives on equities, bonds and currency. Note that the volatility follows a square-root (CIR) process which ensures that the volatility remains non-negative (Albrecher *et al.*, 2006). If the Feller condition holds, i.e. $2\kappa\theta - \sigma^2 \geq 0$, the volatility never reaches zero, almost surely (Kriel, 2014).

The Stochastic Alpha Beta Rho (SABR) model is another novel example of a SV model specified by:

$$dS_t = \alpha S_t^{\beta} dW_t^1$$

$$d\alpha = \nu \alpha dW_t^2$$

and

$$dW_t^1 dW_t^2 = \rho dt\,.$$

This model was designed to fit the observed volatility smile while allowing the skew to move in the same direction as the market level, thus overcoming the drawback of LV models (Hagan *et al.*, 2002). Hagan *et al.* (2002) also argues against the completeness weakness, noting that, in practice, volatility risk can be managed by trading options.

By applying ideas from both SV and LV models, hybrid stochastic local volatility (SLV) models calibrate perfectly to a market smile. This is achieved by multiplying the pure SV component by a leverage function. This leverage function flattens as time passes, and in turn the SLV dynamics show more resemblance to pure SV models. This allows the SLV model to generate a large volatility of volatility and large forward skews, except at the initial time (Guyon, 2014). However, like pure SV models, these are incomplete.

2.4 Path Dependent Volatility Models

In general, a PDV model is of the form

$$\frac{dS_t}{S_t} = rdt + \sigma(t, (S_u, u \leq t))dW_t\,,$$

when ignoring dividends (Guyon, 2014). Discrete time forms of PDV models such as ARCH and GARCH are popular among econometricians, however, they are rarely used in the derivatives industry (Guyon, 2014).

The Hobson-Rodgers model is an early and prominent pure PDV model with the volatility being a deterministic function of $X_t = (X_t^1, ..., X_t^n)$ where X_t^m is the exponentially weighted moments of all the past log increments of the underlying defined by:

$$X_t^m = \int_{-\infty}^{t} \lambda e^{-\lambda(t-u)} \left(ln \frac{S_t}{S_u} \right)^m du\,.$$

For $n = 1$, the volatility depends only on the difference between the current log price and the weighted average of past log prices (Guyon, 2014). Foschi and Pascucci (2008) show that empirical evidence supports this relationship. Furthermore, PDV models of this form do not need to be continuously re-calibrated unlike LV models. Since it incorporates information from the past it accounts for the behaviour of the market, in the case of a market crash it will increase the level of volatility, unlike standard LV and SV models (Foschi and Pascucci, 2008). However, the Hobson-Rodgers model suffers two drawbacks. Firstly, the model considers an infinite time horizon which results in misspecification as only a finite amount of data is available in practice (Foschi and Pascucci, 2008). Secondly, the average weight may not be able to capture the effect of events such as fusion of stocks or capitalisation changes (Foschi and Pascucci, 2008).

Guyon (2014) suggests simpler forms for pure PDV models with the aim of generating the desired spot-vol dynamics and reflecting the past features of volatility. These PDV functions take on one of two specified volatility levels and depend on the current underlying price, S_t, and a specified path-dependent variable, X_t.

In order to fit the oberved market prices, the pure PDV function, $\sigma(t, S_t, X_t)$, is multiplied by a leverage function, $l(t, St)$, yielding the hybrid PDV model:

$$\frac{dS_t}{S_t} = rdt + \sigma(t, S_t, X_t)l(t, S_t)dW_t \,.$$

The calibration of this model involves two components, the choice of the PDV function and the computation of the leverage function. This is done by a Monte Carlo method known as the "particle method" (Guyon and Henry-Labordere, 2012).

By applying Gyöngy's theorem (Appendix A), this model is calibrated perfectly to the volatility smile if and only if:

$$\mathbb{E}^{\mathbb{Q}}[\sigma(t, S_t, X)^2|S_t]l(t, S_t)^2 = \sigma^2_{Dup}(t, S_t)\,,$$

where $\mathbb{Q}$ denotes the risk neutral measure and σ_{Dup} denotes the Dupire local volatility (Guyon, 2014). Hence the model satisfies the non-linear McKean stochastic differential equation:

$$\frac{dS_t}{S_t} = \frac{\sigma(t, S_t, X_t)}{\sqrt{\mathbb{E}^{\mathbb{Q}}[\sigma(t, S_t, X_t)^2|S_t]}}\sigma_{Dup}(t, S_t)dW_t \,. \tag{2.1}$$

A suitable PDV function can be chosen to generate the desired spot-volatility dynamics or to reflect the historic behaviour of volatility. Guyon considers simple choices of the PDV function involving a weighted running average, the minimum, and the maximum of the underlying asset prices over a finite time window. This is illustrated in Tab. 2.1 where

$$\bar{S}_t^{\Delta} = \frac{\int_0^{t-\Delta} \omega_\tau S_\tau d\tau}{\int_0^{t-\Delta} \omega_\tau d\tau}, \quad m_t^{\Delta} = \inf_{t-\Delta \le u \le t} S_u \quad \text{and} \quad M_t^{\Delta} = \sup_{t-\Delta \le u \le t} S_u \,.$$

X_t	$\sigma(S,X)$ for forward skew		$\sigma(S,X)$ for U-shaped forward smile	
$S_{t-\Delta}$	1	$\sigma_H I_{\{\frac{S}{X} \le 1\}} + \sigma_L I_{\{\frac{S}{X} > 1\}}$	4	$\sigma_H I_{\{\lvert\frac{S}{X} - 1\rvert > \kappa\sqrt{\Delta}\}} + \sigma_L I_{\{\lvert\frac{S}{X} - 1\rvert \le \kappa\sqrt{\Delta}\}}$
$\bar{S}_t^{\Delta}$	2	As above	5	As above
$(m_t^{\Delta}, M_t^{\Delta})$	3	$\sigma_H I_{\{\frac{S-m}{M-m} \le \frac{1}{2}\}} + \sigma_L I_{\{\frac{S-m}{M-m} > \frac{1}{2}\}}$	6	$\sigma_H I_{\{\frac{M}{m} - 1 > \kappa\sqrt{\Delta}\}} + \sigma_L I_{\{\frac{M}{m} - 1 \le \kappa\sqrt{\Delta}\}}$

Tab. 2.1: PDV functions adapted from Guyon (2014)

Guyon (2014) provides the intuition behind the formulation of the PDV functions. In order to generate a forward skew, $\sqrt{\eta(t, S_t, X_t)}$ must be negatively correlated with S_t, where

$$\eta(t, S_t, X_t) = \frac{\sigma(t, S_t, X_t^2)}{\mathbb{E}^{\mathbb{Q}}[\sigma(t, S_t, X_t^2) | S_t = S]} \,.$$

Alternatively, in order to generate a forward smile, $\eta(t, S_t, X_t,)$ needs to be highly volatile, uncorrelated with S_t and non-ergodic at the scale of the maturity of the forward smile required. Relating the PDV models to SV models, the spread $\sigma_H - \sigma_L$ influences the volatility of volatility. A larger spread would be able to produce more pronounced skews or smiles. Δ influences the correlation between $\sigma(S_t, X_t)$ and S_t. A small Δ would leave $\sigma(S_t, X_t)$ almost independent of S_t. Note that a (lagged) running average is used in models 2 and 5 in order to preserve the Markov property, as a moving average would not be admissible (Guyon, 2014).

In order to price options, Monte Carlo simulations are used. The process S_t can be discretised by the Euler scheme

$$S_{t+\Delta} = S_t e^{(r - \frac{1}{2}\sigma(S_t, X_t)^2)\Delta + \sigma(S_t, X_t)\sqrt{\Delta} Z} \,, \tag{2.2}$$

where Z is a simulated standard normal random variable. The price of an option can be computed by

$$V_0 = \frac{1}{N} \sum_{i=1}^{N} e^{-rT} \Phi(S_T^i) \,,$$

where $\Phi(S_t)$ is the pay-off function.

For the European call options the pay-off function is defined as

$$\Phi_{K,T}(S_T) = (S_T - K)^+$$

and for European put options the pay-off function is defined as

$$\Phi_{K,T}(S_T) = (K - S_T)^+ ,$$

with strike K and maturity T.

Guyon (2014) also notes that the PDV models could even be further generalised to include path dependent interest rates and dividend yields, while maintaining completeness. The model would then follow the following dynamics:

$$\frac{dS_t}{S_t} = (r_t - q_t)dt + \sigma_t l(t, S_t)dW_t ,$$

where $r_t = r(t, (S_u, u \leq t)), q_t = q(t, S_t, u \leq t))$ and $\sigma_t = \sigma(t, (S_u, u \leq t))$ are all path dependent. In this dissertation, only path-dependency for the volatility is considered.

Chapter 3

Model Calibration

This chapter details the implementation of the PDV models for vanilla European call options on the JSE FTSE Top 40 index. This is preceded by a discussion of the data used in this dissertation and the calibration of the Black-Scholes, CEV and Heston models, which are used for comparison against the PDV models.

The calibration of the parameters is performed by the least squares method. There are several options available using either the price or the implied volatility surface, with either an absolute or relative error. No significant differences are expected between the various options. In this dissertation, the price surface with an absolute error is used. We define the sum of squared errors (SSE) by the squared difference between the fitted option price and the observed market option price, summed over all strikes and maturities.

$$SSE = \sum_K \sum_T [C(T,K) - C(\hat{T},K)]^2 \,,$$

where $C(\hat{T},K)$ are the fitted values of the option prices for the given set of parameters. Note that this is an unweighted SSE, hence each strike and maturity is given equal importance in the calibration procedure. The parameters are tuned by minimising the SSE through an iterative procedure.

3.1 Data

The JSE FTSE Top 40 is the most widely used index on the South African market for derivatives. It includes the 40 largest companies listed on the JSE, weighted by free float market capitalisation. In order to calibrate the models for use with instruments based on this index, an implied volatility surface based on the index is required. In the South African market, vanilla European options are liquidly traded on the JSE, with the implied volatility of the contracts being quoted. However, these options are only traded with standardised maturities and strikes. Interpola-

tion and extrapolation of the implied volatility surface is therefore required for a full calibration over a wider range of strikes and maturities. In this dissertation, complete volatility surfaces, obtained from industry practitioners, for 31 Mar 2016, 28 Apr 2016, 31 May 2016, 30 Jun 2016, 29 Jul 2016 and 1 Sep 2016 are used. The strikes considered range from 60% moneyness to 123% moneyness, in increments of mostly 2.5%. The maturities considered start from 1 month and increase with an increment of a month, up until 60 months. Thereafter the maturities increase in 6 month intervals, up until 120 months. A risk-free rate of 7% is used, together with a zero dividend yield. This risk-free rate was chosen to reflect the market conditions which prevailed over the period in consideration.

3.2 Black-Scholes

The Black-Scholes model requires the calibration of a single parameter, namely the constant volatility level. The analytical price for a vanilla European option is used, given by

$$C(T,K) = S_0 N(d_+) - Ke^{-rT} N(d_-)$$

where

$$d_\pm = \frac{ln(\frac{S_0}{K}) + (r \pm \frac{1}{2}\sigma^2)T}{\sigma\sqrt{T}}\,, \tag{3.1}$$

and $N(.)$ denotes the cumulative distribution function of the standard normal distribution (Hull, 2006). The SEE behaviour is illustrated for the different choices of the constant volatility below in Figure 3.1 and the calibration results are illustrated in Table 3.1.

	Mar 2016	Apr 2016	May 2016	Jun 2016	Jul 2016	Aug 2016	Mean
σ	21%	21%	21%	21%	21%	20%	-
SSE	0.1247	0.1309	0.1513	0.2182	0.1325	0.1460	0.1506

Tab. 3.1: Calibration of Black-Scholes Model

3.3 CEV Model

The CEV model requires two parameter estimates, σ and α. The closed form prices for European call options are used, given by:

$$C(T,K) = S_0[1 - \mathcal{P}(y,z,x)] - Ke^{-rT}\mathcal{P}(x,z-2,y)\,,$$

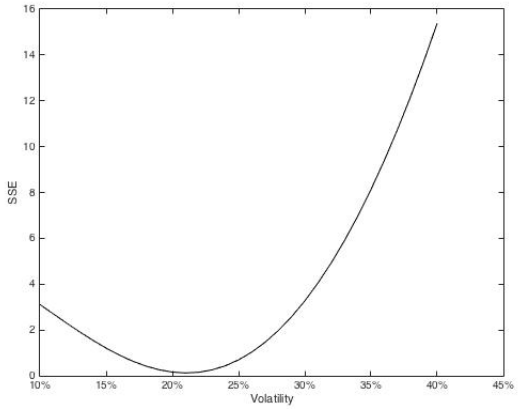

Fig. 3.1: Calibration of Black-Scholes Model at Mar 2016

where

$$\kappa = \frac{2r}{\sigma^2(1-\alpha)(e^{2r(1-\alpha)T}-1)}$$

$$x = \kappa S_0^{2(1-\alpha)} e^{2r(1-\alpha)T}$$

$$y = \kappa K^{2(1-\alpha)}$$

and

$$z = 2 + \frac{1}{1-\alpha}$$

where $\mathcal{P}(., d, \lambda)$ denotes the non-central chi-square distribution with d degrees of freedom and non-centrality parameter λ. The behaviour of the SSE with respect to the parameters is illustrated in Figure 3.2 and the calibration results are summarised in Table 3.2.

	Mar 2016	Apr 2016	May 2016	Jun 2016	Jul 2016	Aug 2016	Mean
σ	21%	21%	21%	22%	21%	21%	-
α	−0.03	−0.04	−0.01	0.06	0.00	0.04	-
SSE	0.0512	0.0551	0.0734	0.1096	0.0614	0.0795	0.0717

Tab. 3.2: Calibration of CEV Model

Note that some of the calibrations provided negative alpha parameters. The CEV model is classically defined with a non-negative alpha value (Cox, 1975). However, this constraint is not enforced here. Jackwerth and Rubinstein (2001)

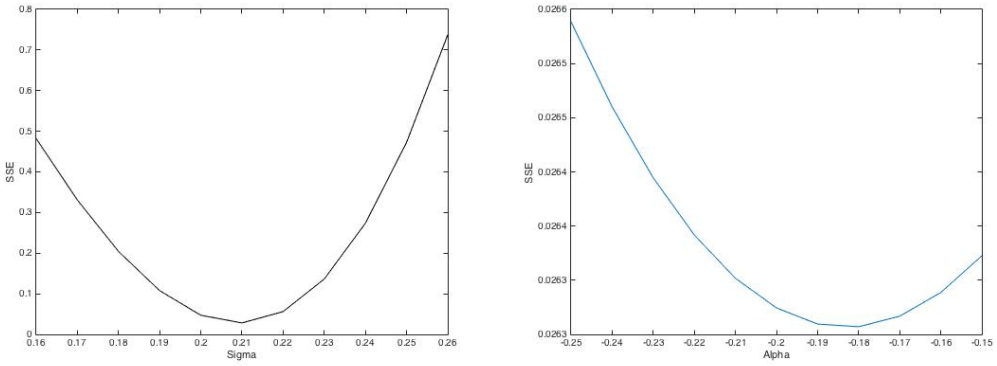

(a) σ **(b)** α

Fig. 3.2: Calibration of CEV Model at Mar 2016

refer to this as the unrestricted CEV model, and note that although it may have undesirable economic implications, it is mathematically legitimate. In the equity index options market, negative alpha values are typical and implicit in market prices (Davydov and Linetsky, 2001).

3.4 Heston Model

The calibration of the Heston stochastic volatility model involves the estimation of five parameters, v_0, κ, θ, σ, and ρ. For computation of the option prices, semi-analytical formulae are available.

$$C(T,k) = S_0 P_1 - K P_2 \,,$$

with quadrature approximations for the two probabilities

$$P_1 = \frac{1}{2} + \frac{1}{\pi} \sum_{n=1}^{N} Re\Big[\frac{e^{-iu_n k}\phi_{s_T}(u_n - i)}{iu_n \phi_{s_T}(-i)}\Big]\Delta u$$

and

$$P_2 = \frac{1}{2} + \frac{1}{\pi} \sum_{n=1}^{N} Re\Big[\frac{e^{-iu_n k}\phi_{s_T}(u_n)}{iu_n}\Big]\Delta u \,,$$

where $u_n = (n - \frac{1}{2})\Delta u$, with the integration range being truncated to the interval $[0, u_{max}]$ and $\Delta u = \frac{u_{max}}{N}$

The number of quadrature steps used to calibrate the model is $N = 100$ with an upper integration limit of $u_{max} = 30$. For numerical stability, the 'Little Trap' specification for the characteristic function is employed (Albrecher *et al.*, 2006).

$$\phi_{s_T}(u) = e^{C+Dv_0+iuln(S_0)},$$

where

$$C = rTiu + \theta\kappa(Tx - -\frac{1}{a}ln(\frac{1-ge^{-Td}}{1-g}))$$

and

$$D = \frac{1-e^{-Td}}{1-ge^{-Td}}x_-$$

with

$$a = \frac{\sigma^2}{2}$$

$$b = \kappa - \rho\sigma iu$$

$$c = -\frac{u^2+iu}{2}$$

$$d = \sqrt{b^2-4ac}$$

$$x_\pm = \frac{b \pm d}{2a}$$

and

$$g = \frac{x_-}{x_+}.$$

The behaviour of each of the parameters with respect to the SSE is illustrated below in Figure 3.3 and the calibration results are summarised in Table 3.3.

	Mar 2016	Apr 2016	May 2016	Jun 2016	Jul 2016	Aug 2016	Mean
v_0	0.06	0.05	0.03	0.06	0.04	0.02	-
κ	3.59	3.75	3.69	4.09	3.76	3.62	-
θ	0.05	0.05	0.05	0.05	0.05	0.05	-
σ	1.93	1.91	1.88	1.90	1.87	1.81	-
ρ	-0.27	-0.30	-0.28	-0.44	-0.29	-0.24	-
SSE	0.0126	0.0117	0.0141	0.0192	0.0116	0.0188	0.0147

Tab. 3.3: Calibration of Heston Model

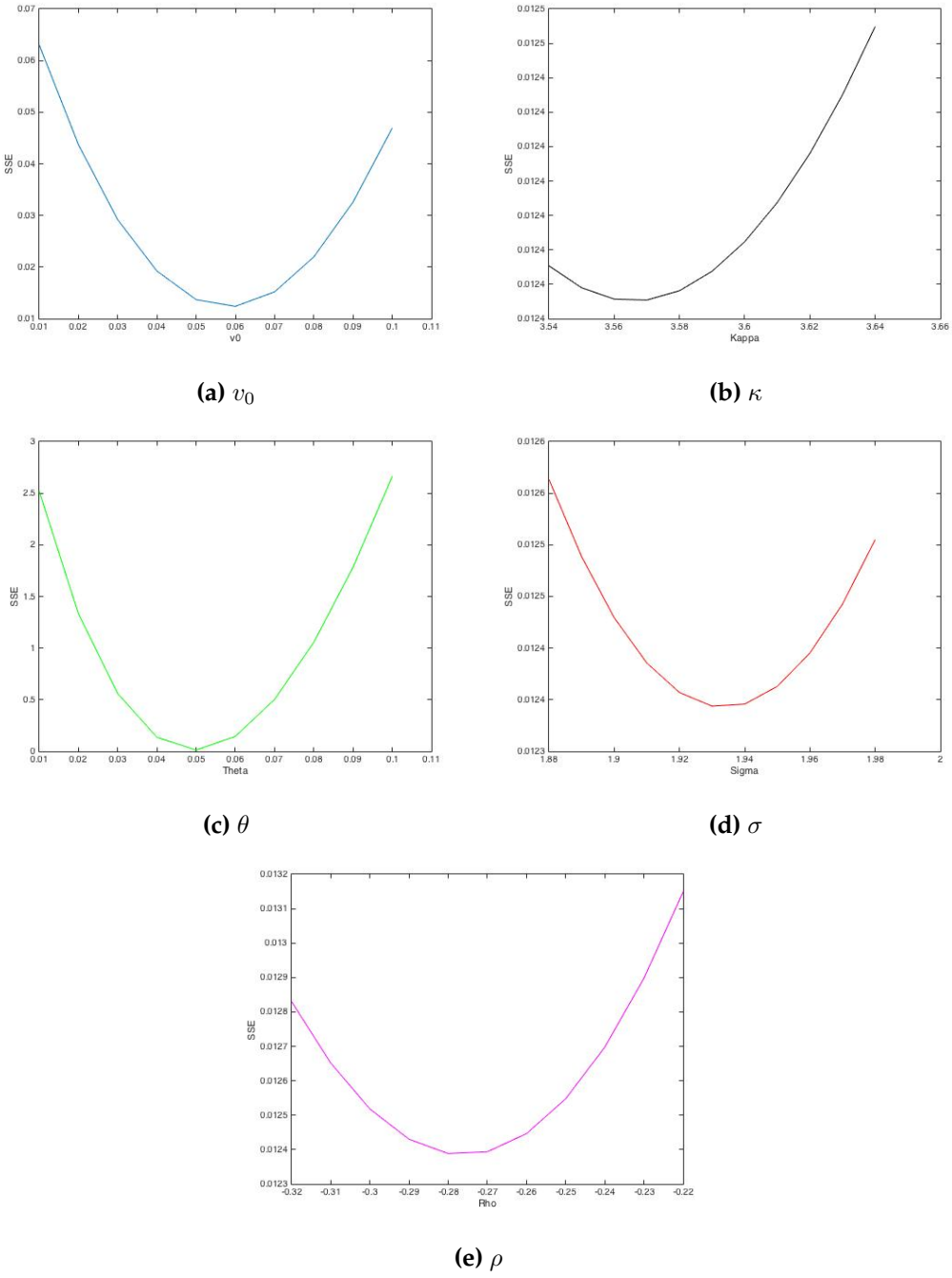

(a) v_0 **(b)** κ

(c) θ **(d)** σ

(e) ρ

Fig. 3.3: Calibration of Heston Model at Mar 2016

Note that the calibrated set of parameters do not meet the Feller conditions in all cases, and was not enforced in the calibration. Cui *et al.* (2017) note that the Feller condition is often violated in practice as relaxing the constraint is not only harmless for modelling, but can even be beneficial for pricing.

3.5 Pure PDV Models

For PDV models 1-3, two parameter estimates are required, namely the low and high volatility levels. For models 4-6, an additional parameter estimate is required, namely κ, which determines the discontinuity point of the PDV function i.e. the point at which the volatility level changes. In this dissertation, Δ, the time lag, is kept constant at one month. Variation of the Δ will influence the time discretisation used for the Monte Carlo simulation. Here, a monthly time discretisation is used for computational convenience. For models 2 and 5, an equal weighting, $\omega_t = 1$, is assigned to the running average of the underlying process.

The parameter set is selected according to

$$(\sigma_H, \sigma_L, \kappa) = \underset{\sigma_H, \sigma_L, \kappa}{\arg\min} \sum_K \sum_T [C(T,K) - C(\hat{T},K)]^2 .$$

For each of the six examples of pure PDV models considered, the parameter calibration routine is performed, thus selecting the optimum parameter set for each of the models.

Hereafter the best fitting PDV model, PDV model 2, will be referred to Pure PDV 2. The parameter tuning for Pure PDV 2 is illustrated below in Figure 3.4 and the results are summarised in Table 3.4.

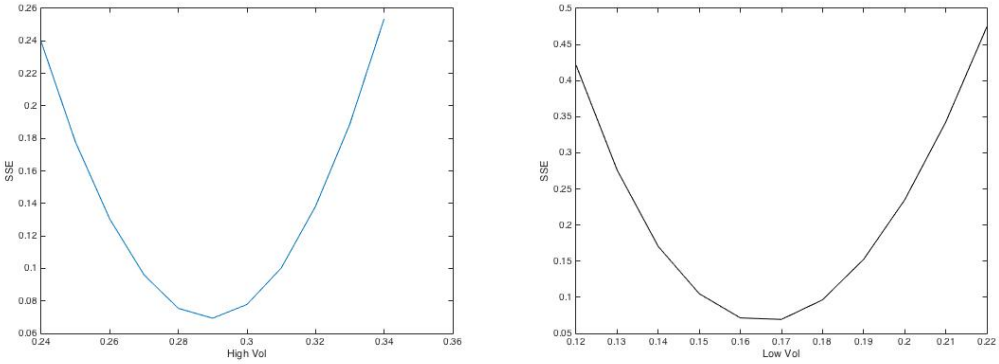

(a) σ_H **(b)** σ_L

Fig. 3.4: Calibration of Pure PDV 2 at Mar 2016

3.6 Hybrid PDV Models

Although the calibration of hybrid PDV models is detailed here for completeness, these models are not used in this dissertation. The leverage function calibration

	Mar 2016	Apr 2016	May 2016	Jun 2016	Jul 2016	Aug 2016	Mean
σ_H	29%	29%	28%	29%	29%	27%	-
σ_L	17%	16%	17%	17%	17%	17%	-
SSE	0.0694	0.0744	0.0920	0.1021	0.0783	0.0941	0.0850

Tab. 3.4: Calibration of Pure PDV 2

can be performed using the 'particle method' (Guyon and Henry-Labordere, 2011). This is a Monte-Carlo type method which is optimised for efficiency. The conditional expectation in Equation 2.1 is estimated during the simulation of the asset price path.

First, the time interval $[0, T]$ is discretised to the set $\{t_k\}$. Consider a grid $G_{S,t}$ of values for S and a threshold η. The steps for the algorithm follow:

1. Initialise k=1 and set $l(t, S) = \frac{\sigma_{Dup}(0,S_0)}{\sigma(0,S_0,X_0)}$ for all t
2. Simulate the N processes $\{S_t^{i,N}, \sigma(t, S_t, X_t)\}_{i=1,\dots,N}$ from t_{k-1} to t_k
3. Sort the simulations according to the asset price. For $S \in G_{S,t_k}$ find the smallest index $i_-(S)$ and the largest index $i^-(S)$ for which $\delta_{t_k,N}(S_{t_k}^{i,N} - S) > \eta$ and compute the leverage function

$$l(t_k, S) = \sigma_{Dup}(t_k, S) \sqrt{\frac{\sum_{i=i_-(S)}^{i^-(S)} \delta_{t_k,N}(S_{t_k}^{i,N} - S)}{\sum_{i=i_-(S)}^{i^-(S)} \sigma(t_k, S_{t_k}, X_{t_k})^2 \delta_{t_k,N}(S_{t_k}^{i,N} - S)}} \,,$$

where a regularisation kernel $\delta_{t,N}$ is used instead of the Dirac Delta. The regularisation kernel suggested by Guyon and Henry-Labordere (2011) is defined by

$$\delta_{t,N}(x) = \frac{1}{h_{t,N}} K(\frac{x}{h_{t,N}})$$

$$h_{t,N} = \kappa S_0 \sigma_{VS,t} \sqrt{\max(t, t_{\min})} N^{-\frac{1}{5}}$$

and

$$K(x) = \frac{15}{16}(1 - x^2)^2 I_{|x|\leq 1} \,,$$

where $\sigma_{VS,t}$ is the variance swap volatility at time t. Guyon and Henry-Labordere (2011) suggest $\kappa \simeq 1.5$ and $t_{\min} = \frac{1}{4}$.

Interpolate the leverage function with cubic splines and extrapolate it flat outside the interval $[\min(G_{S,t_k}), \max(G_{S,T_k})]$. Set $l(t,S) = l(t_k,S)$ for all $t \in [t_k, t_{k+1}]$.

4. Set $k = k + 1$ and iterate through steps 2 and 3 up to the maturity date T.

Chapter 4

Results

This chapter first details the results of the pricing and hedging tests for the PDV models, with Black-Scholes, CEV and Heston model benchmarks for comparison. Thereafter the results for the pricing of forward starting options are presented.

4.1 Pricing

In this section, each model is calibrated and then used to price European call options over the full range of maturities and strikes. The pricing test is performed with different calibration frequencies. Firstly, a monthly calibration is used, with lower frequencies tested subsequently. The errors are standardised by setting the initial underlying price to 1 (essentially re-basing the index) and using strikes as a percentage of the underlying price (moneyness). A 7% risk-free rate and zero dividend yield is used. The pricing errors are illustrated with respect to the maturities and strikes in Figure 4.2. Examples of the implied volatility surfaces generated by the different models used are illustrated below in Figure 4.3. Note that the implied volatility surfaces generated from the models may not be arbitrage-free due to the nature of the input data used for calibration (Homescu, 2011). This is observed with implied volatility of the Heston model.

Three different calibration frequencies are tested:

- Monthly: Each model is calibrated and then used to price options in the following month
- Bi-monthly: Each model is calibrated and then used to price options in the second following month
- Tri-monthly: Each model is calibrated and then used to price options in the third following month

The SSE between the model generated prices and the actual market prices, over all strikes and maturities, is tabulated in Table 4.1 below.

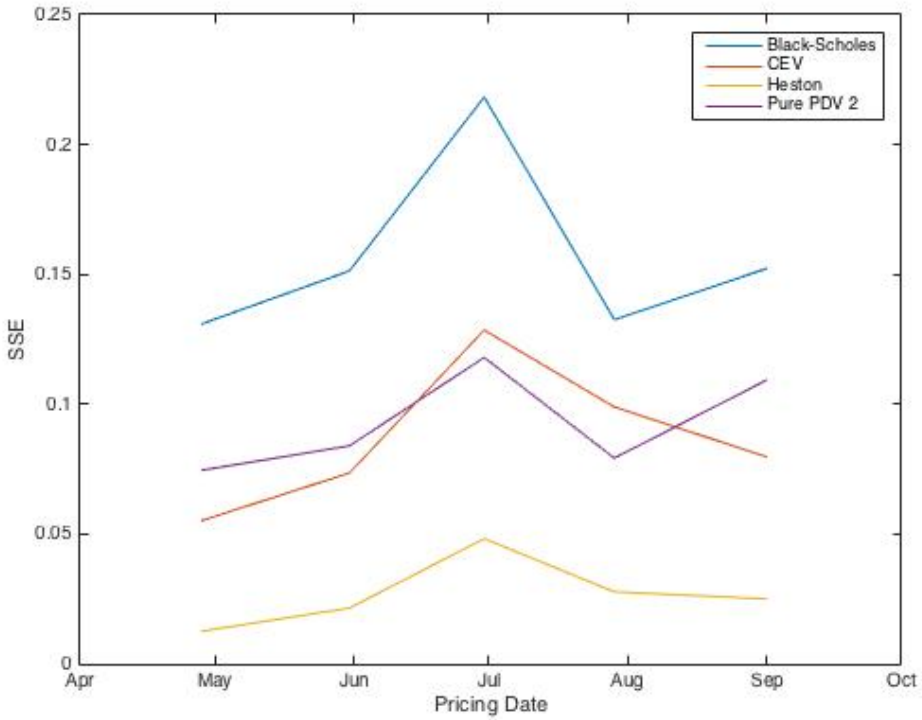

(a) Monthly

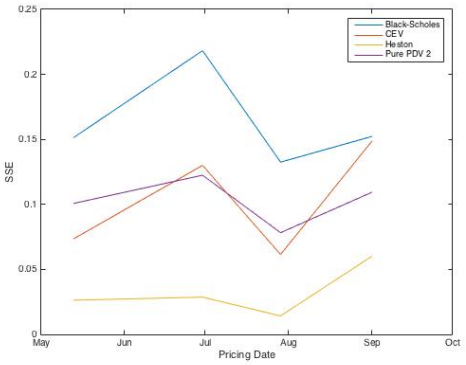

(b) Bi-monthly

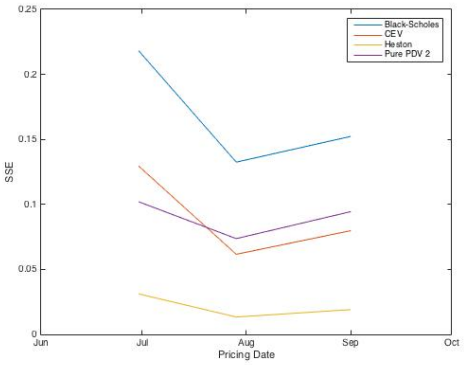

(c) Tri-monthly

Fig. 4.1: Pricing Error

4.2 Hedging

4.2.1 Delta-Hedging

Here delta hedging using the PDV model is tested against the Black-Scholes, Heston and CEV models. Note that this test is subject to bias from the actual index

Model	Monthly	Bi-monthly	Tri-monthly
Black-Scholes	0.1570	0.1636	0.1677
CEV	0.0872	0.1034	0.0903
Heston	0.0270	0.0323	0.0212
Pure PDV 2	0.0930	0.1027	0.0900

Tab. 4.1: Average Pricing Error over Testing Period

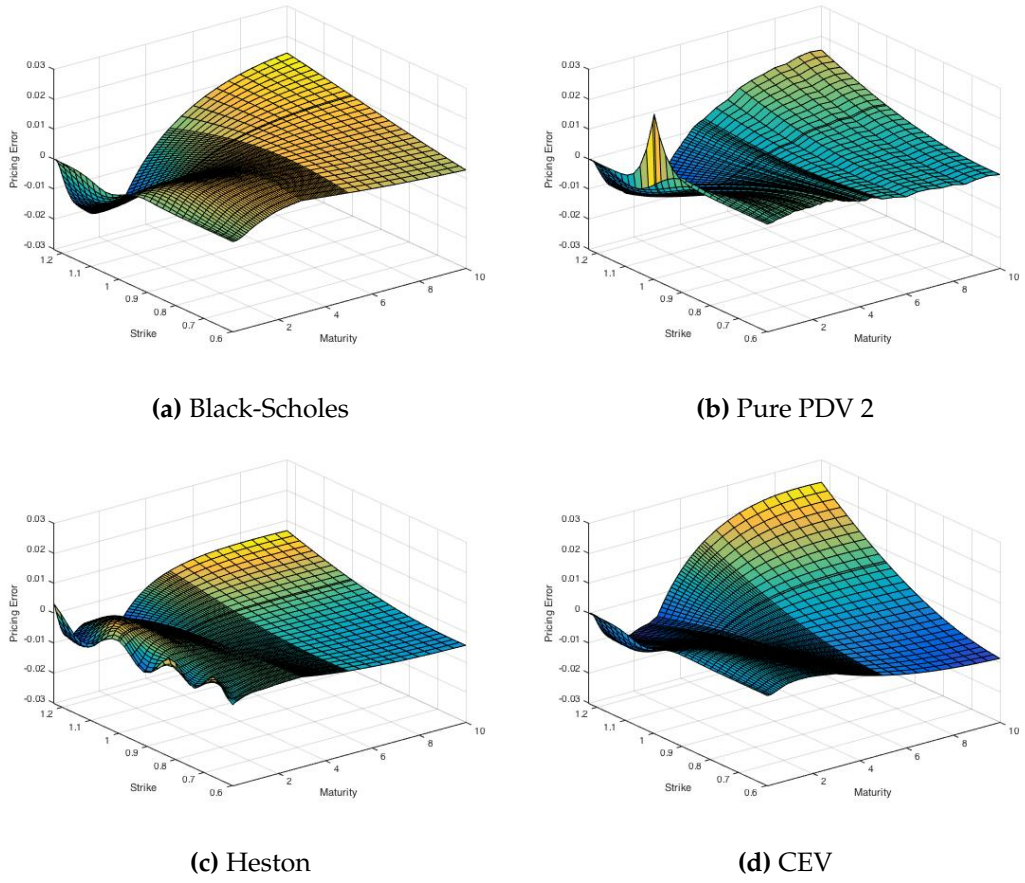

(a) Black-Scholes

(b) Pure PDV 2

(c) Heston

(d) CEV

Fig. 4.2: Pricing Error for Apr 2016 with Monthly Calibration

performance over the time period considered in this paper. Hedged portfolios using both vanilla European call and put options are tested.

Static Delta Hedging

First, a static delta hedge is considered. At the initial time, 31 Mar 2016, the procedure is detailed below.

For the call options:

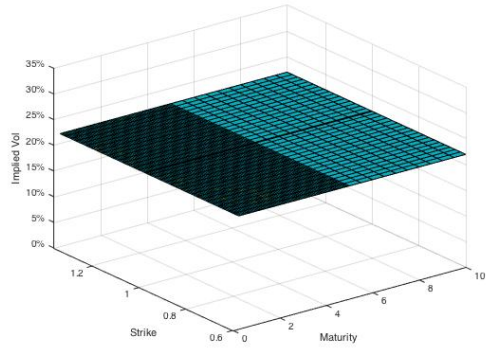

(a) Black-Scholes

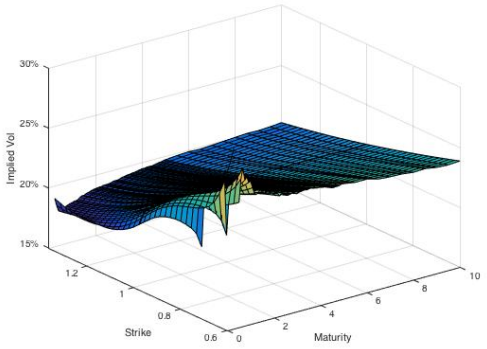

(b) Pure PDV 2

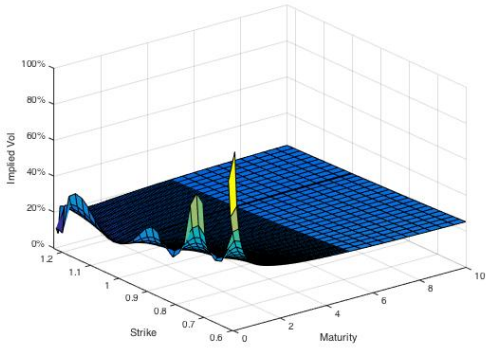

(c) Heston

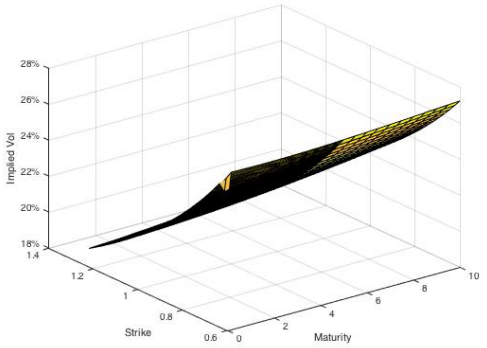

(d) CEV

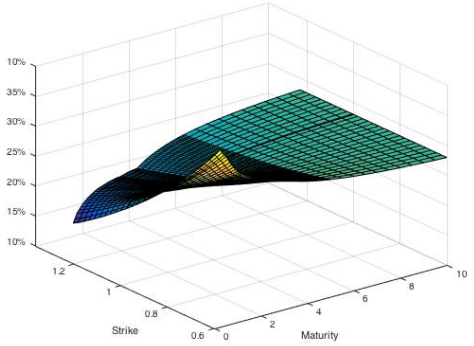

(e) Observed Market

Fig. 4.3: Implied Volatilities Generated by Calibrated Models at Mar 2016

1. Set up delta-neutral portfolios by shorting a European call option and longing Δ units of the underlying (re-based to one). Therefore the initial portfolio value is:

$$\Pi_0 = C(T, K) - \Delta \times S_0 \,,$$

where Δ_C is defined as

$$\Delta_C = \frac{\partial C(T,K)}{\partial S}$$

2. Calculate the profit and loss (P&L) at each of the maturity dates for which market data is available.

$$\Pi_T = \Pi_0 \times e^{rT} + \Delta_C \times S_T - \Phi_{K,T}(S_T)\,,$$

where $\Phi(x)_{K,T} = x - K$ is the pay-off function for the European call option with strike K and maturity T

For the put options:

1. Set up delta-neutral portfolios by longing a European put option and longing $|\Delta_P|$ units of the underlying (re-based to one). Therefore the initial portfolio value is:

$$\Pi_0 = -P(T,K) - |\Delta_P| \times S_0\,,$$

where the Δ_P is defined as

$$\Delta_P = \frac{\partial P(T,K)}{\partial S}$$

2. Calculate the P&L at each of the maturity dates for which market data is available.

$$\Pi_T = \Pi_0 \times e^{rT} + |\Delta_P| \times S_T + \Phi_{K,T}(S_T)$$

where $\Phi(x)_{K,t} = K - x$ is the pay-off function for the European put option with strike K and maturity T

For the Black-Scholes model, the delta for a vanilla European call is given by the analytical expression:

$$\Delta_C = N(d_+)\,,$$

where d_+ is as defined in equation 3.1 and $N(.)$ is the cumulative distribution function of the standard normal distribution (Hull, 2006). Similarly, for vanilla European put options the Black-Scholes delta is given by:

$$\Delta_P = N(d_+) - 1\,.$$

However, for the PDV, Heston and CEV models, a finite difference is used to approximate the derivative:

$$\Delta_C = \frac{C(T,K,S_0+\delta_S) - C(T,K,S_0-\delta_S)}{2 \times \delta_S}$$

and

$$\Delta_P = \frac{P(T, K, S_0 + \delta_S) - P(T, K, S_0 - \delta_S)}{2 \times \delta_S},$$

with $\delta_S = 1\%$.

The P&L obtained using the delta from each of the considered models is illustrated for hedged portfolios using calls puts in Table 4.2, where the P&L is averaged over all strikes and maturity dates.

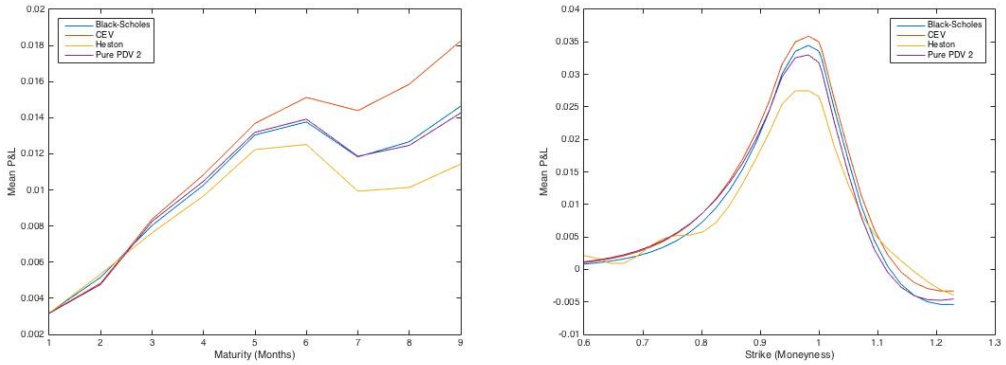

(a) By maturity, averaged over all strikes **(b)** By strike, averaged over all maturities

Fig. 4.4: P&L of Statically Hedged Call portfolios

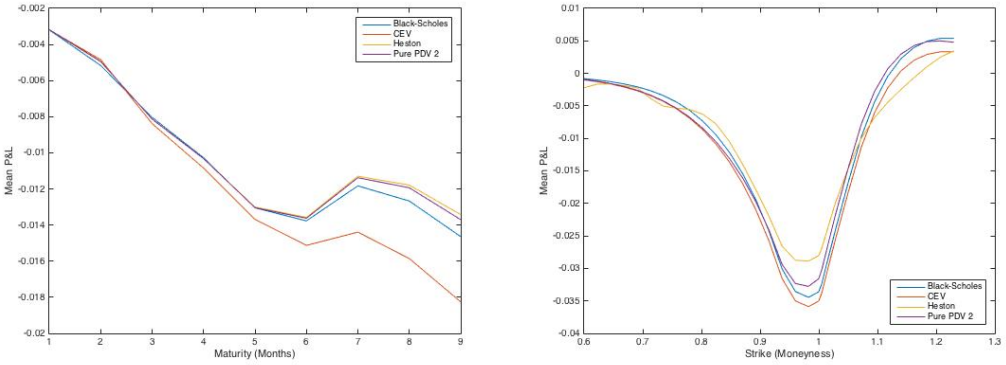

(a) By maturity, averaged over all strikes **(b)** By strike, averaged over all maturities

Fig. 4.5: P&L of Statically Hedged Put Portfolios

Dynamic Delta Hedging

In the previous test, the portfolios were statically hedged at the initial date. Here, the test is extended to a dynamically hedged portfolio. Although dynamic hedging

Model	Calls	Puts
Black-Scholes	0.0103	−0.0103
CEV	0.0116	−0.0116
Heston	0.0091	−0.0100
Pure PDV 2	0.0103	−0.0100

Tab. 4.2: Mean P&L of Statically Delta-hedged Portfolios from 31 Mar 2016

is highly regarded in classic literature, Ahn and Wilmott (2008) outline the problems with this method. For this test a delta-neutral portfolio is set up at the initial time, 31 Mar 2016. The portfolios are then rebalanced to maintain delta neutrality at each of the dates for which data is available. The portfolio values are rolled up to each hedging date and rebalanced as:

$$\Pi_{t_t} = \Pi_{t_{i-1}} \times e^{r(t_i - t_{t-1})} - (|\Delta_{t_i}| - |\Delta_{t_{i-1}}|) \times S_{t_i} \,,$$

where t_i denotes the current hedging date, t_{i-1} denotes the previous hedging date, $\Delta_{t_{i-1}}$ denotes the delta calculated at the previous hedging date (using the parameters calibrated at the previous hedging date) and Δ_{t_i} denotes the delta calculated at the current hedging date (using the parameters calibrated at the current hedging date).

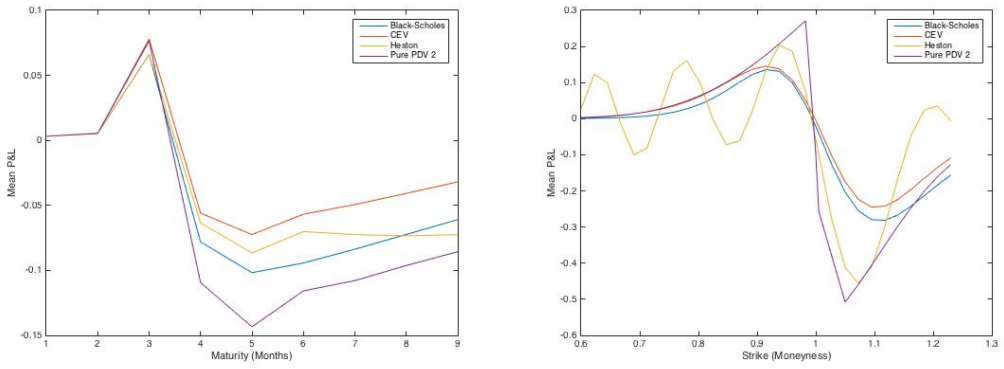

(a) By maturity, averaged over all strikes **(b)** By strike, averaged over all maturities

Fig. 4.6: P&L of Dynamically Hedged Call portfolios

Delta Sensitivity to Volatility Shocks

In this test, a shock is applied to the market implied volatilities. Using the initial date of 31 Mar 2016 as the reference time, the entire volatility surface is scaled up by a factor of β and the models are re-calibrated. The deltas are then recalculated and

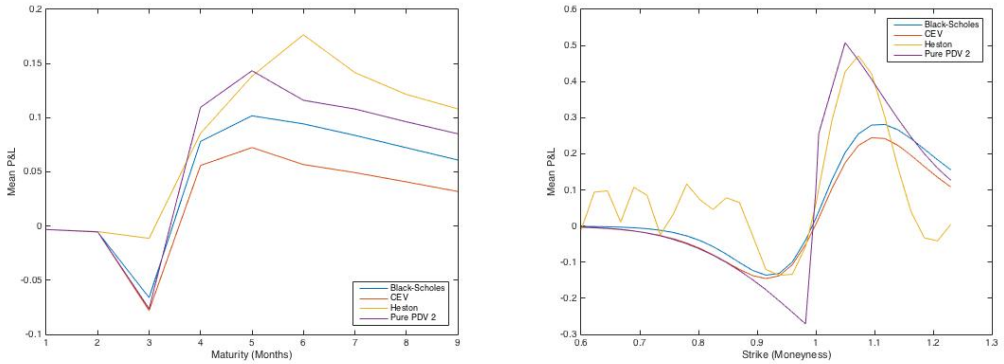

(a) By maturity, averaged over all strikes **(b)** By strike, averaged over all maturities

Fig. 4.7: P&L of Dynamically Hedged Put Portfolios

Model	Calls	Puts
Black-Scholes	−0.0463	0.0463
CEV	−0.0245	0.0245
Heston	−0.0401	0.0836
Pure PDV 2	−0.0637	0.0637

Tab. 4.3: Mean P&L of Dynamically Delta-hedged Portfolios from 31 Mar 2016

compared to the original deltas. This gauges the sensitivity of the deltas to volatility shocks experienced in the market. The squared differences are also calculated and summed over all maturities and strikes as:

$$\sum_K \sum_T (\Delta'_{K,T} - \Delta_{K,T})^2 \,,$$

where $\Delta'_{K,T}$ denotes the delta after the shock is applied and $\Delta_{K,T}$ denotes the original delta, for maturity T and strike K.

The differences are illustrated in Figure 4.8 and the squared differences are summarised in Table 4.4.

Model	$\beta = 1.1$	$\beta = 1.2$
Black-Scholes	0.2513	1.3233
CEV	0.7003	2.5751
Heston	2.8354	5.3878
Pure PDV 2	0.3433	1.1982

Tab. 4.4: Total Squared Delta Difference from Volatility Shocks

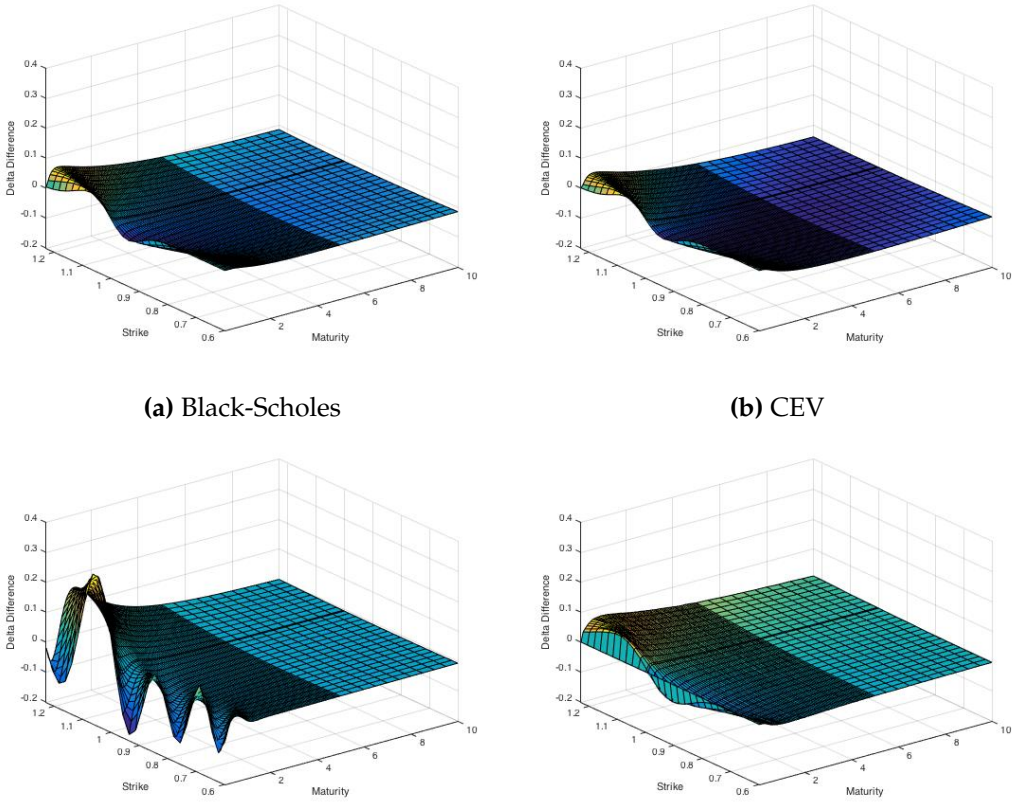

(a) Black-Scholes

(b) CEV

(c) Heston

(d) Pure PDV 2

Fig. 4.8: Delta Differences from Volatility Shocks

Comparison Against Sticky Delta

The difference between the delta generated from each of the models and the delta calculated from the implied volatility surface prevailing in the market (known as the sticky delta) is illustrated in Figure 4.9 (Foschi and Pascucci, 2008).

As a additional comparison metric, the SSE between the delta obtained from the models and the sticky delta is used. This is summarised in Table 4.10, with different calibration frequencies.

Model	Monthly	Bi-monthly	Tri-monthly
Black-Scholes	1.1293	1.1835	1.2327
CEV	5.3348	5.5772	5.5126
Heston	5.7860	5.8243	5.755
Pure PDV 2	2.8348	2.9302	3.0127

Tab. 4.5: Mean SSE between Model Generated Delta and Sticky Delta

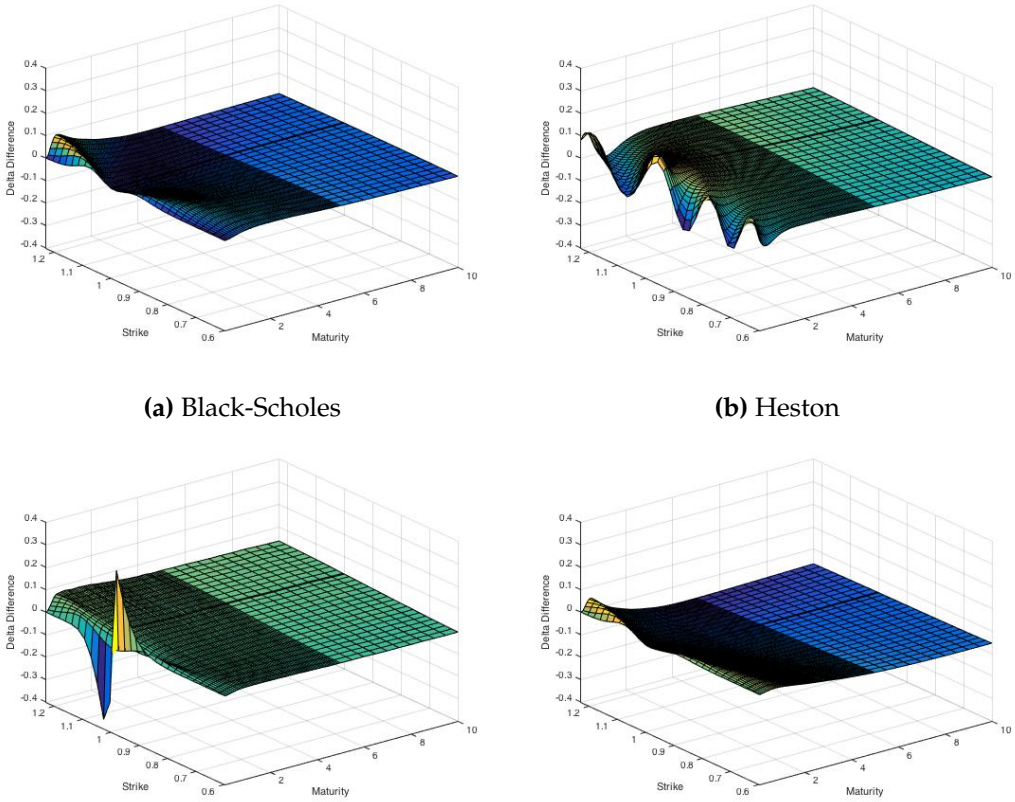

(a) Black-Scholes

(b) Heston

(c) Pure PDV 2

(d) CEV

Fig. 4.9: Difference Between Deltas and Sticky Deltas at Mar 2016

4.2.2 Gamma

The Gamma of an option is defined by

$$\Gamma = \frac{\partial C(T,K)}{\partial S^2} = \frac{\partial \Delta}{\partial S}\,.$$

This Greek measures the sensitivity of an option's delta with respect to the underlying asset price (Hull, 2006). Gamma hedged portfolios P&L are not tested here. Instead, only the Black-Scholes gamma calculated from the market implied volatility surface (referred to as the sticky gamma) is compared with the model output. This is illustrated in Figure 4.11 with the SSE summarised in Figure 4.12 and Table 4.6 for different calibration frequencies. For the Black-Scholes model, the closed form expression for the gamma is given by

$$\Gamma = \frac{\phi(d_+)}{S_0\sigma\sqrt{T}}\,,$$

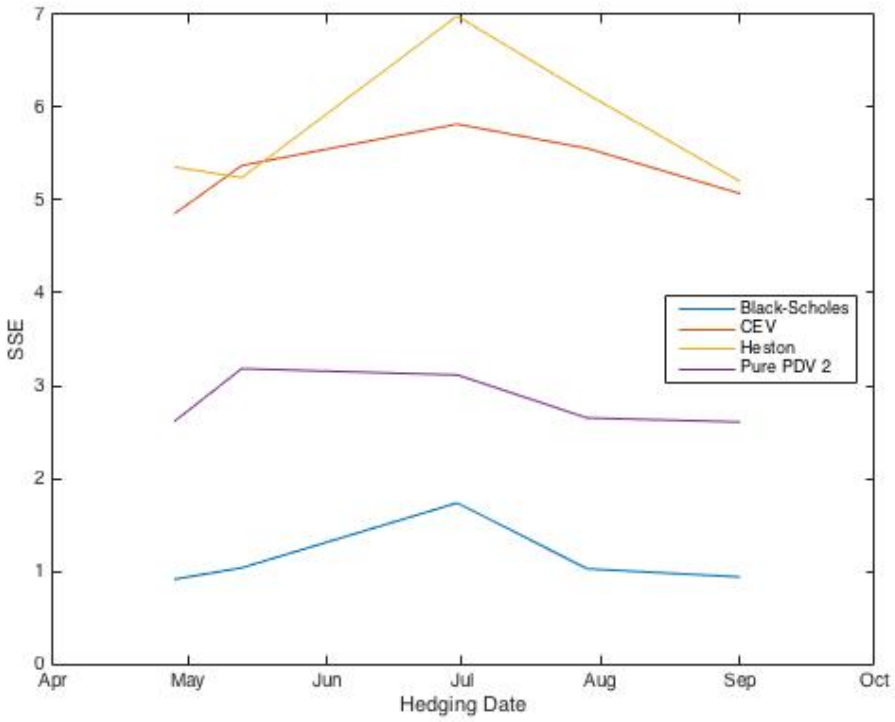

(a) Monthly

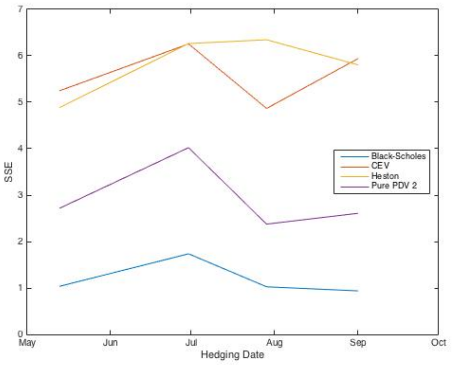

(b) Bi-monthly

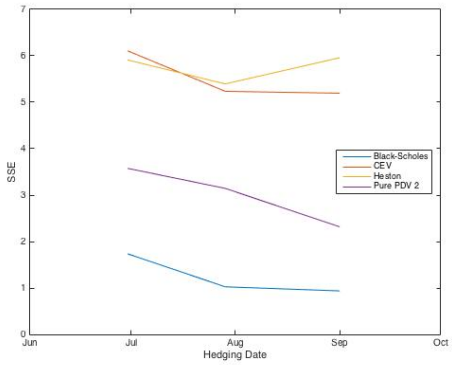

(c) Tri-monthly

Fig. 4.10: SSE between Model Generated Delta and Sticky Delta

where $\phi(.)$ denotes the probability density function for the standard normal distribution. For the other models, a finite difference approximation is used

$$\Gamma = \frac{C(T, K, S_0 + 2\delta_S) - 2C(T, K, S_0) + C(T, K, S_0 - 2\delta_S)}{4\delta_S^2},$$

with $\delta_S = 1\%$.

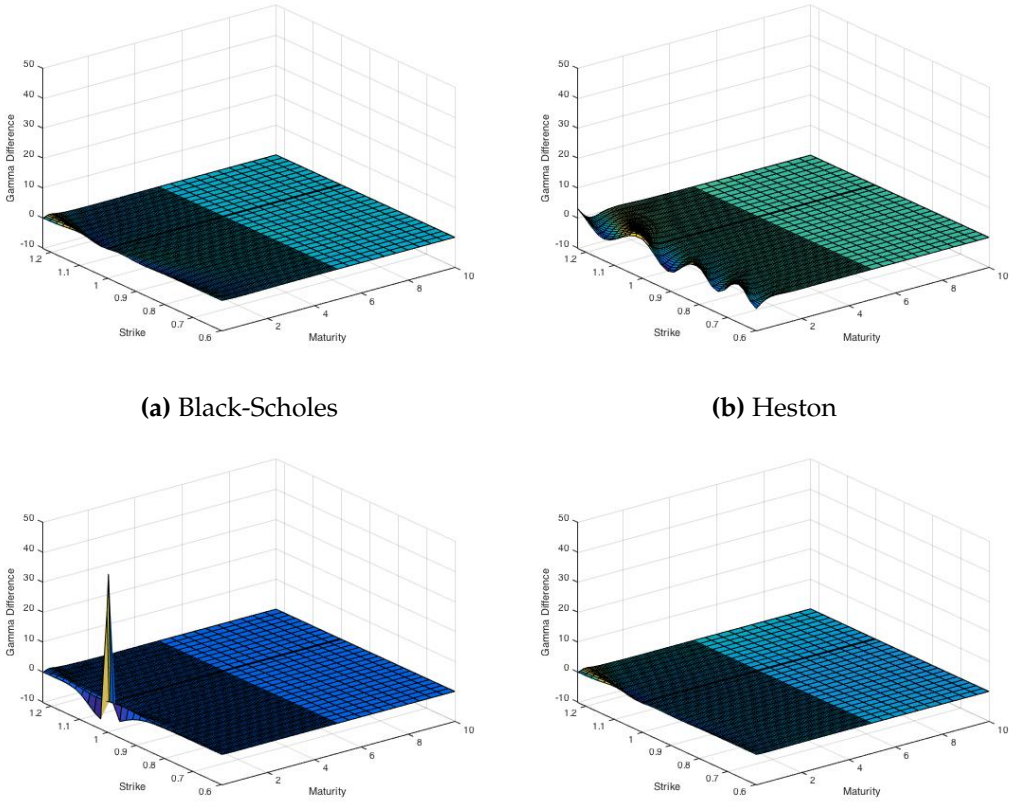

(a) Black-Scholes

(b) Heston

(c) Pure PDV 2

(d) CEV

Fig. 4.11: Difference Between Gamma and Sticky Gamma at Mar 2016

Model	Monthly	Bi-monthly	Tri-monthly
Black-Scholes	63.7783	69.2104	67.5296
CEV	54.4557	61.6258	56.2116
Heston	781.4557	743.6530	773.0335
Pure PDV 2	2 308.9244	2 146.6096	1 903.4996

Tab. 4.6: Mean SEE between Model Generated Gamma and Sticky Gamma

4.3 Forward Starting Options

This section serves as an extension to the dissertation. While the preceding results were based on market data, here prices for these simple exotic options are not available as these instruments are not exchange traded. Hence only the model generated prices for the PDV, Black-Scholes and Heston models are compared. Consider a forward starting call option on the JSE Top 40 index with maturity T, with the strike determined ATM at time t^*. The payoff function is given by

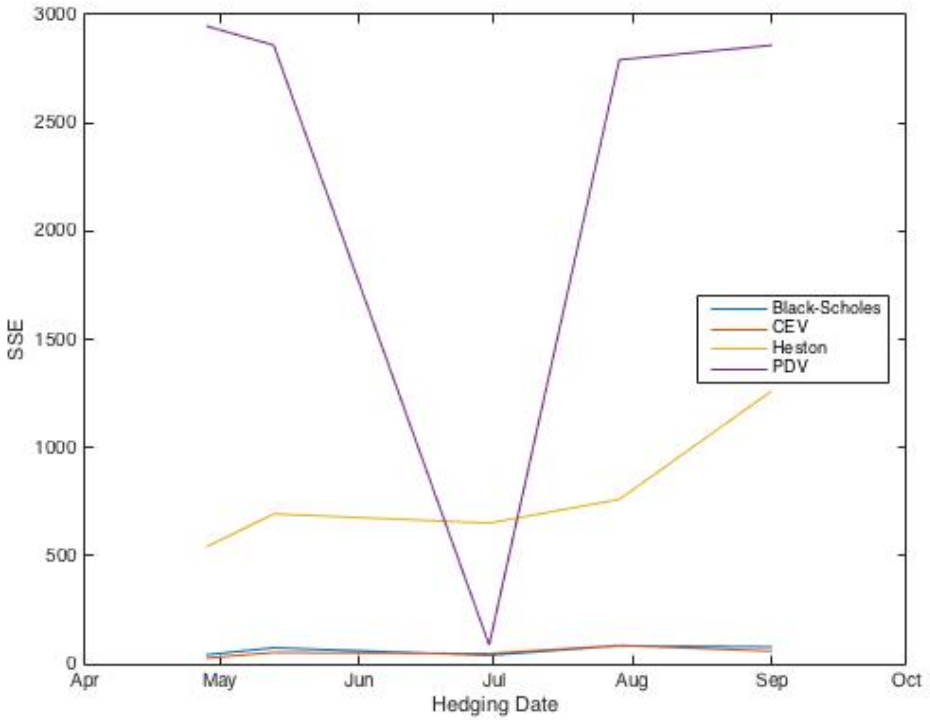

(a) Monthly

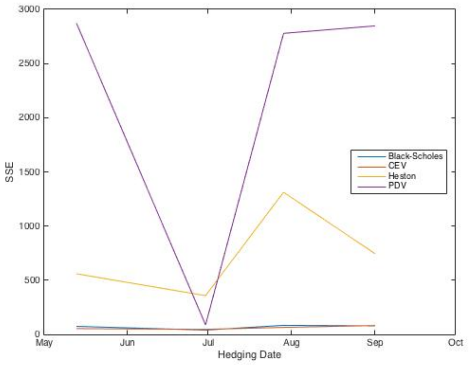

(b) Bi-monthly

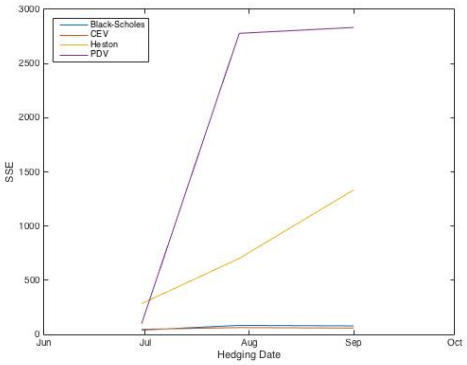

(c) Tri-monthly

Fig. 4.12: SEE between Model Generated Gamma and Sticky Gamma

$$\Phi(S_T) = (S_T - S_{t^*})^+ .$$

In the Black-Scholes model, where volatility, and hence forward volatility is constant, the analytical price of this option is given by

$$C = S_0[N(d_+) - e^{-r(T-t^*)}N(d_-)]$$

with

$$d_+ = \frac{(r - \frac{1}{2}\sigma^2)(T - t^*)}{\sigma\sqrt{T - t^*}}$$

and

$$d_- = d_+ - \sigma\sqrt{T - t^*}\,.$$

Wilmott (2002) describes the risks associated with the constant volatility assumption for these types of exotic options. For the PDV and Heston models, a Monte Carlo simulation is used to compute the price, with the Euler discretisation scheme for the PDV model, as given by Equation 2.2. A Milstein scheme used for the Heston model given by

$$S_{t+\Delta} = S_t e^{(r-\frac{1}{2}v_t)\Delta + \sqrt{v_t\Delta}Z_s}$$

and

$$v_{t+\Delta} = (v_t + \kappa(\theta - v_t)\Delta + \sigma\sqrt{v_t\Delta}Z_v + \frac{1}{4}\sigma(Z_v - 1)\Delta)^+\,,$$

where Z_s and Z_v are standard normal random variables with correlation ρ.

All prices are calculated using a 7% risk-free rate, zero dividend yield and the calibrated parameters for 31 Mar 2016. The prices of these options for different specifications of T and t^* are detailed in Table 4.7.

Model	$T = 1, t^* = \frac{1}{2}$	$T = 2, t^* = 1$	$T = 5, t^* = 2$	$T = 10, t^* = 5$
Black-Scholes	0.0770	0.1190	0.2463	0.3466
Heston	0.0971	0.1553	0.3174	0.4250
Pure PDV 2	0.0781	0.1179	0.2438	0.3382

Tab. 4.7: Forward Starting Call Prices

In Figure 4.13 the behaviour of prices when fixing the strike determination date and the maturity date is illustrated.

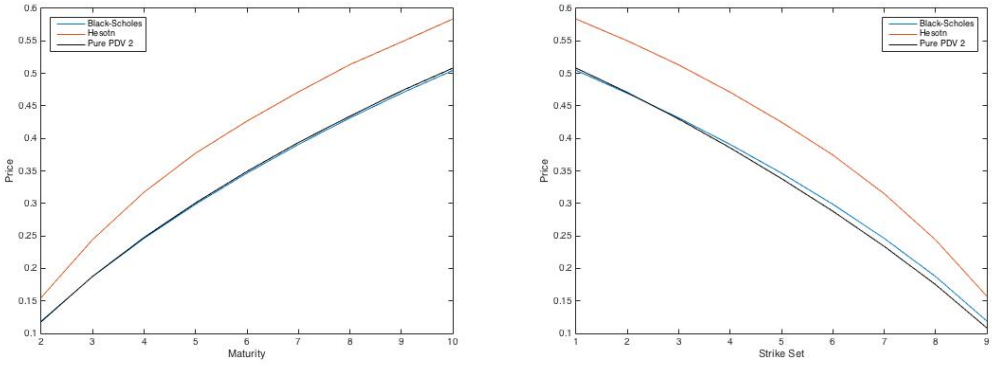

(a) Fixed $t^* = 1$ **(b)** Fixed $T = 10$

Fig. 4.13: Forward Starting Option Prices with respect to t^* and T

Chapter 5

Discussion and Conclusion

In this section the results presented in the previous chapter are discussed and the concluding remarks are presented.

From the model calibration, one observes that the parameters for the PDV models are relatively stable, compared to the Heston SV model.

In terms of the pricing results, the PDV model clearly outperforms the constant volatility Black-Scholes model. However, the PDV model is not able to price as accurately as the Heston model. The PDV model performs well against the CEV model, especially as the calibration becomes less frequent. All the models considered show overpricing of long dated, out-the-money (OTM) European call options. There is also a uniform underpricing of 2-4 year OTM call options, across all models. The notable differences in the model generated prices were found at the short maturities. It is evident that a large contributor to the total error for the PDV models can be attributed to the short maturity, at-the-money (ATM) options. While the metric used for comparison in this dissertation was the SSE across a wide range of strikes and maturities, for some practitioners it may be more useful to restrict the comparison to smaller subsets of strikes and maturities.

In terms of hedging, the P&L of the delta-hedged portfolios reflect similar results for the calls and put portfolios. With a complete hedge, one would expect a P&L of zero, therefore the deviation from this expected value provides insight into the hedge effectiveness. In the static hedge setting, the Heston model produced the most effective hedge for the call portfolios and outperformed the PDV model. The Black-Scholes model matched the mean P&L of the PDV model for call portfolios, however, for the put portfolios, the PDV model outperformed, matching the Heston model's performance. In both cases the PDV model clearly outperforms the CEV model. Moving to the dynamic hedge setting, the CEV model unexpectedly produced the most effective hedge for both call and put portfolios. The dynamically hedged portfolios performed worse than the statically hedged portfolios, which is even more counter-intuitive. The PDV model proved to be ineffective

for this type of hedging scenario and only outperformed the Heston model for put portfolios. It must be noted that these results are consequences of the actual market performance. An appropriate extension for this would therefore be to implement this test under different periods of market performance, as well as to extend it into a more frequently dynamically hedged portfolio, rather than the sparse discrete hedging tested here. The PDV model deltas proved to be robust under volatility shocks, showing the lowest difference for the largest shock tested. In contrast, the Heston model deltas proved to be the most unstable under volatility shocks. The comparison between the model generated delta and gamma, with the sticky delta and gamma provide a qualitative comparison, however, no conclusive measure of true hedge effectiveness can be drawn from this metric. A notable feature of the PDV model is the spike for the ATM short maturity delta and gamma difference.

The results from the forward option pricing reflect that the PDV model yields similar prices as the Black-Scholes model when the period between the strike date and maturity is small. However, as this period increases in length, the PDV price falls below the Black-Scholes price. The Heston model prices were significantly higher than both the PDV and Black-Scholes prices for all specifications considered.

In conclusion, the PDV models perform remarkably well against the Black-Scholes constant volatility model. It also fares well against the CEV LV and Heston SV model. Although the Heston model still outperforms the PDV models for pricing across the full range of considered maturities and strikes, it is worth noting the relative simplicity of the PDV model, as well as the loss of completeness in the stochastic volatility framework. Another possible extension of this dissertation is the adaptation of the pricing and hedging tests to include the hybrid PDV models which are able to calibrate to the market smile exactly. A notable drawback of the pure PDV models was the under-performance for short maturity, ATM options. Hence, to further improve the performance of the pure PDV models used here, the calibration could rather involve a weighted SSE minimisation, with a higher weighting given to ATM options. Practitioners indicate that the most liquid options are those with a maturity of up to 3 years and a strike between 80% and 120%. This range could therefore be given a higher weighting. In addition, a calibration using the implied volatility surface could rather be employed. Lastly, a finer discretisation for the PDV Monte Carlo simulations could be investigated, as opposed to the monthly discretisation used here.

Bibliography

Ahn, H. and Wilmott, P. (2008). Dynamic Hedging is Dead! Long Live Static Hedging, *Wilmott* pp. 80–87.

Albrecher, H., Mayer, P., Schoutens, W. and Tistaert, J. (2006). The Little Heston Trap.

Black, F. and Scholes, M. (1973). The Pricing of Options and Corporate Liabilities, *The Journal of Political Economy* pp. 637–654.

Cox, J. (1975). Notes on Option Pricing: Constant Elasticity of Variance Diffusions, *Stanford University, Graduate School of Business* .

Cui, Y., del Baño Rollin, S. and Germano, G. (2017). Full and Fast Calibration of the Heston Stochastic Volatility Model, *European Journal of Operational Research* .

Davydov, D. and Linetsky, V. (2001). Pricing and Hedging Path-dependent Options Under the CEV Process, *Management Science* **47**(7): 949–965.

Derman, E. (2003). Laughter in the Dark - The Problem of the Volatility Smile, *Euronext Options Conference (Amsterdam)*.

Dumas, B., Fleming, J. and Whaley, R. E. (1998). Implied Volatility Functions: Empirical Tests, *The Journal of Finance* **53**(6): 2059–2106.

Dupire, B. *et al. (1994). Pricing With a Smile,* Risk **7***(1): 18–20.*

Foschi, P. and Pascucci, A. (2008). Path Dependent Volatility, Decisions in Economics and Finance **31***(1): 13–32.*

Guyon, J. (2014). Path-dependent Volatility.

Guyon, J. and Henry-Labordere, P. (2011). The Smile Calibration Problem Solved.

Guyon, J. and Henry-Labordere, P. (2012). Being Particular About Calibration, Risk .

Gyöngy, I. (1986). Mimicking the One-dimensional Marginal Distributions of Processes Having an Itô Differential, Probability Theory and Related Fields **71***(4): 501–516.*

Hagan, P. S., Kumar, D., Lesniewski, A. S. and Woodward, D. E. (2002). Managing Smile Risk, The Best of Wilmott *p. 249.*

Harrison, J. M. and Pliska, S. R. (1981). Martingales and Stochastic Integrals in the Theory of Continuous Trading, Stochastic Processes and Their Applications **11***(3): 215–260.*

Heston, S. L. (1993). A Closed-form Solution for Options With Stochastic Volatility With Applications to Bond and Currency Options, Review of Financial Studies **6***(2): 327–343.*

Hobson, D. G. and Rogers, L. (1998). Complete Models With Stochastic Volatility, Mathematical Finance **8***(1): 27–48.*

Homescu, C. (2011). Implied Volatility Surface: Construction Methodologies and Characteristics.

Hull, J. (2006). Options, Futures, and Other Derivatives, *Pearson Education.*

Hull, J. and White, A. (1987). The Pricing of Options on Assets With Stochastic Volatilities, The Journal of Finance **42***(2): 281–300.*

Jackwerth, J. C. and Rubinstein, M. (2001). Recovering Stochastic Processes from Option Prices.

Kriel, H. (2014). Volatility Derivatives in the Heston Framework, *Master's thesis, University of Cape Town.*

Linetsky, V. and Mendoza, R. (2010). Constant Elasticity of Variance (CEV) Diffusion Model, Encyclopedia of Quantitative Finance .

Merton, R. C. (1973). Theory of Rational Option Pricing, The Bell Journal of Economics and Management Science *pp. 141–183.*

Romano, M. and Touzi, N. (1997). Contingent Claims and Market Completeness in a Stochastic Volatility Model, Mathematical Finance **7***(4): 399–412.*

Wilmott, P. (2002). Cliquet Options and Volatility Models, The Best of Wilmott *p. 379.*

Appendix A

Gyöngy's Theorem

Let ϵ_t be a stochastic process with Itô differential

$$d\epsilon_t = \beta(t, w)dt + \delta(t, w)dW_t$$

where W_t is a Wiener process, ϵ and β are bounded processes such that $\delta\delta^T$ is uniformly positive definite. Then there exists a stochastic differential equation

$$dX_t = b(t, x(t))dt + \sigma(t, x(t))dW_t$$

with non-random coefficients which admits a weak solution X_t having the same one-dimensional probability distribution as ϵ_t for every t with

$$\sigma(t, x) = \sqrt{\mathbb{E}[\delta\delta^T(t)|\epsilon_t = x]}$$

and

$$b(t, x) = \mathbb{E}[\beta(t)|\epsilon_t = x]$$

For the proof see Gyöngy (1986).

Appendix B

FTSE JSE Top 40 Index

The index values used in the hedging test is detailed below in Table B.1 and the movement is illustrated in Figure B.1.

Time Point	Date	Published Index Value	Re-based Index
1	31 Mar 2016	46 139.99	1.0000
2	29 Apr 2016	46 471.00	1.0072
3	31 May 2016	47 974.09	1.0398
4	30 Jun 2016	45 974.31	0.9964
5	29 Jul 2016	45 916.48	0.9952
6	31 Aug 2016	46 261.02	1.0026
7	30 Sep 2016	45 425.59	0.9845
8	31 Oct 2016	44 019.39	0.9540
9	30 Nov 2016	43 691.42	0.9469
10	30 Dec 2016	43 901.99	0.9515

Tab. B.1: FTSE JSE Top 40 Published Index and Re-based Index

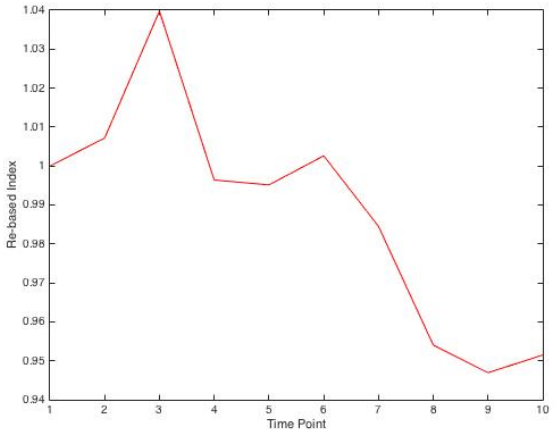

Fig. B.1: Re-based Index over 31 Mar 2016 to 30 Dec 2016